

Lattice Genons

Zhao Liu,¹ Gunnar Möller,^{2,3,*} and Emil J. Bergholtz⁴

¹*Dahlem Center for Complex Quantum Systems and Institut für Theoretische Physik,
Freie Universität Berlin, Arnimallee 14, 14195 Berlin, Germany*

²*Functional Materials Group, School of Physical Sciences, University of Kent, Kent CT2 7NZ, United Kingdom*

³*TCM Group, Cavendish Laboratory, University of Cambridge, Cambridge CB3 0HE, United Kingdom*

⁴*Department of Physics, Stockholm University, AlbaNova University Center, 106 91 Stockholm, Sweden*

(Dated: December 3, 2024)

Topological degeneracy is, together with fractionalization, the hallmark of topological order. While fractionalization has been demonstrated both theoretically and in laboratories leading to deep insights into our basic understanding of matter, there has been no corresponding success in tracking the evolution of ground-state degeneracy due to the lack of tractable microscopic models with arbitrarily tunable topology of space. In this work however, by computer simulations, we show that lattice versions of multicomponent fractional quantum Hall systems are novel playgrounds to fill this void. With wormhole-like defects that connect separated “universes” of different components, thus changing the global topology of space, we observe a nontrivial dependence of ground-state degeneracy on the number of defects, equivalent to adding exotic non-Abelian quasiparticles called “genons” proposed recently in terms of effective topological field theory. We identify a number of different lattice genons in both Abelian and non-Abelian phases, with quantum dimensions exceeding those of fundamental quasiparticles in the host states, and provide a promising platform to study their intriguing behavior.

Topologically ordered phases of matter have been a central theme of condensed matter physics in the last decades for both fundamental research [1–10] and technological development [11, 12]. A remarkable fingerprint of topological order is the robust ground-state degeneracy, being insensitive to local details but crucially depending on the global topology of space [1, 2]. However, a comprehensive study of this dependence on variable topologies was for long challenging in both computer simulations and experiments. Taking two-dimensional systems as an example, the most accessible setups in laboratories only have planar geometry with zero genus. Although the situation could be slightly improved in computer simulations, where various microscopic models can be easily adapted to periodic boundary conditions leading to a torus geometry with unit genus, further progress was extremely difficult due to the lack of tractability of arranging these models on surfaces with higher genus.

A crucial step forward was made in Ref. [13], in which it was proposed that appropriate defects in the system can effectively increase the genus of space, thus enabling us to track the enhancement of topological degeneracy by adding such defects, even though the original system only has planar geometry. These defects, which were further predicted to carry nontrivial quantum dimensions and obey projective braiding statistics, can be imagined as a new type of extrinsic non-Abelian quasiparticle called “genon” [14]: they are different from intrinsic quasiparticles of the host system, thus extending our knowledge of topological order and opening a new possibility of quantum computation. However, this beautiful idea is only based on effective topological field theory, and its actual relevance to microscopic models remains open.

In this letter, we fill this void by presenting the first evidence of genons in a microscopic lattice model which can favor lattice versions of fractional quantum Hall states, i.e., fractional Chern insulators [15, 16], and naturally host de-

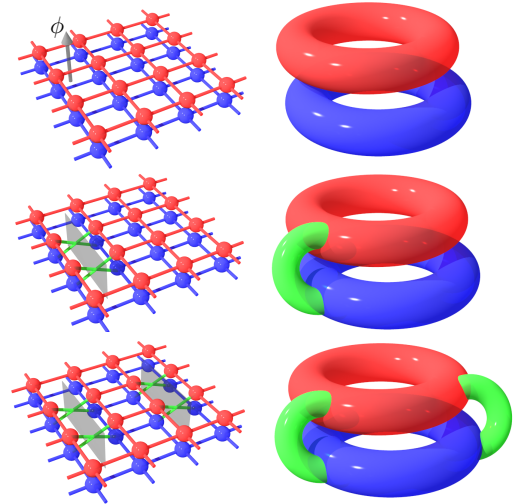


Figure 1. Lattice model, defects, branch cuts and the corresponding topologies. Our model is equivalent to two square lattice layers (blue and red) where each plaquette is pierced by an effective flux ϕ (upper left panel). Defects are introduced through branch cuts (transparent grey) where the particles switch layer (green). We study systems with up to two such branch cuts corresponding to the topologies displayed in the right panel.

fects. With compelling results from computer simulations of exact diagonalization, we explicitly demonstrate the dependence of ground-state degeneracy on the genus of space effectively tuned by lattice defects to high numbers. Our results provide a deep insight into the physical realization of genons in realistic lattice models and open the experimental accessibility of topological orders on high-genus surfaces.

Our model (see Appendix ‘Tight-binding Hamiltonian’) is located on a two-dimensional square lattice with two internal degrees of freedom $\sigma = \uparrow, \downarrow$ on each lattice site and an ef-

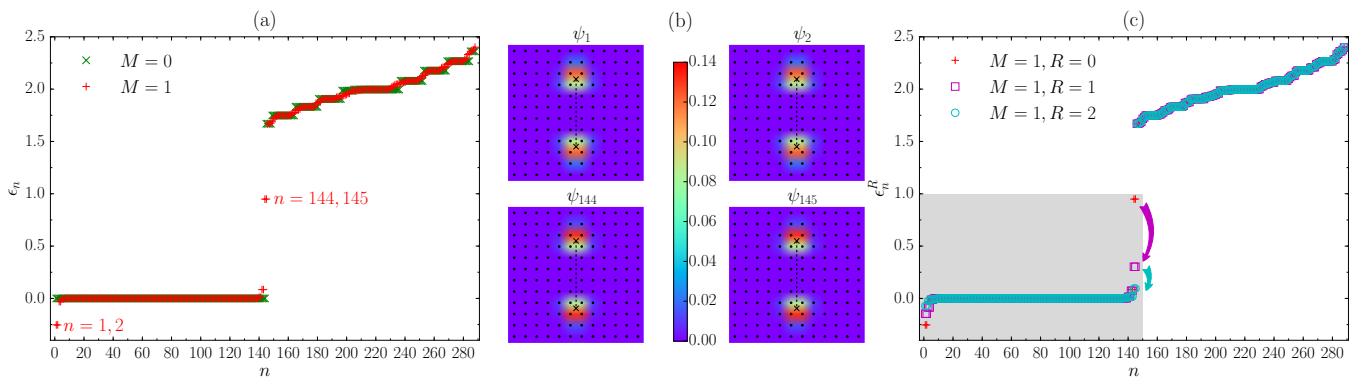


Figure 2. Single-particle spectra and defect-induced localized states. We study the band structure on a $L_x \times L_y = 12 \times 12$ lattice with $\phi = 1/2$. (a) The single-particle spectrum $\{\epsilon_n\}$ of H_0 . In the absence of defects ($M = 0$), $\epsilon_1, \dots, \epsilon_{144}$ are exactly degenerate at zero energy. With one pair of defects ($M = 1$) at $(5.5, 2.5 \rightarrow 8.5)$, the original band structure is distorted, with two nearly degenerate clusters (ϵ_1, ϵ_2) and ($\epsilon_{144}, \epsilon_{145}$) having the largest deviation. (b) The lattice site weight of eigenvectors $\psi_1, \psi_2, \psi_{144}, \psi_{145}$ of H_0 for the same defects as in (a). All of them are strongly localized near the defects. The eigenstates with less energy deviation from the original band structure, for example, $\psi_3, \psi_4, \psi_{142}, \psi_{143}$, are less localized (not shown here). (c) The single-particle spectrum $\{\epsilon_n^R\}$ of $H_0 + V$ with $R = 0, 1$, and 2 and the same defects as in (a). $\epsilon_1^R, \dots, \epsilon_{145}^R$ which we must flatten (shaded in gray) becomes more degenerate for larger R , with the flatness $0.6, 3.1, 9.4$ for $R = 0, 1, 2$.

fective magnetic flux $\phi = 1/q$ piercing each elementary plaquette, with q integer (Fig. 1). For convenience, we refer to the internal degree of freedom as “layer”. In the absence of lattice defects, our model has Z_2 symmetry associated with exchanging two layers, and its lowest band structure contains two copies of an exactly flat band at zero energy with Chern number $\mathcal{C} = 1$ [17].

In the following, we introduce a specific class of defects into the lattice, which can be considered as Z_2 twist defects [14] in the sense that a particle’s layer index is flipped when it moves around such a defect once. It is helpful to imagine that the layer flipping occurs precisely along a branch cut between a pair of defects. In case a straight hopping line intersects with n branch cuts, the particle flips its layer index n times. Without loss of generality (see Appendix ‘Tilted branch cuts’), we arrange a pair of defects at (X_1, Y_1) and (X_1, Y_2) with a branch cut denoted as $(X_1, Y_1 \rightarrow Y_2)$ along the y -direction (Fig. 1). Under periodic boundary conditions in both x and y directions, the topology of our model strongly depends on the number of branch cuts (Fig. 1). Each branch cut plays a role of a wormhole connecting two tori [13], hence the presence of M branch cuts leads to a surface with genus $g = M + 1$.

We first diagonalize the tight-binding Hamiltonian H_0 on a periodic lattice of $L_x \times L_y$ sites to analyze the effect of defects on the band structure. We assume that L_x is divisible by q ensuring integer number of unit cells in the x -direction. In the absence of defects, the lowest $2\phi L_x L_y$ single-particle energy levels are exactly degenerate at zero energy. Such a flatness is distorted by the presence of M pairs of defects, and we identify $4M$ levels with the most significant deviation from the original band structure: $2M$ of them (levels $\epsilon_1, \dots, \epsilon_{2M}$) drop below the original lowest band, and another $2M$ ($\epsilon_{2\phi L_x L_y - M + 1}, \dots, \epsilon_{2\phi L_x L_y + M}$) move into the orig-

inal lowest band gap. Moreover, they form nearly degenerate clusters respectively. An example of the band structure for $M = 1$ is shown in Fig. 2(a). We further examine the eigenvectors of these $4M$ levels. Remarkably, we find that all of them are strongly localized near the defects [Fig. 2(b)], and the localization becomes weaker (or completely disappears) for other levels with less deviation from the original band structure. This localization enables us to do a controlled tuning of deviated energies by local potentials near the defects without significantly distorting the rest of the band structure, as we explain below.

Next we consider $N_b = \frac{k}{2}(2\phi L_x L_y)$ bosons interacting via $(k + 1)$ -body onsite repulsions

$$H_{\text{int}} = \sum_{i \in \mathcal{L}, \sigma = \uparrow, \downarrow} : n_{i,\sigma} n_{i,\sigma} \cdots n_{i,\sigma} : \quad (1)$$

on the lattice \mathcal{L} , where $k \geq 1$ is an integer. In this setup, the ground state in the absence of defects is two copies of model \mathcal{Z}_k Read-Rezayi (RR) states on the lattice, which reside in the lowest $2\phi L_x L_y$ exactly degenerate eigenstates of H_0 with filling fraction $\nu = N_b / (2\phi L_x L_y) = k/2$ [18, 19]. Adding defects should not change the filling fraction in the thermodynamic limit, hence the most promising candidate of the ground state for M pairs of defects is the \mathcal{Z}_k RR state on a single $g = M + 1$ surface, residing in the lowest N_s eigenstates of H_0 with the same filling fraction $\nu = \lim_{N_b \rightarrow \infty} N_b / N_s = k/2$. In accordance with this we target

$$N_s = 2N_b/k - (1 - g) \quad (2)$$

which also agrees with the continuum prediction in the lowest Landau level [20, 21]. The extra offset $1 - g$ is related to a topological quantity called the “shift”. To amplify the effect of the interaction, we consider the limit of N_s degenerate

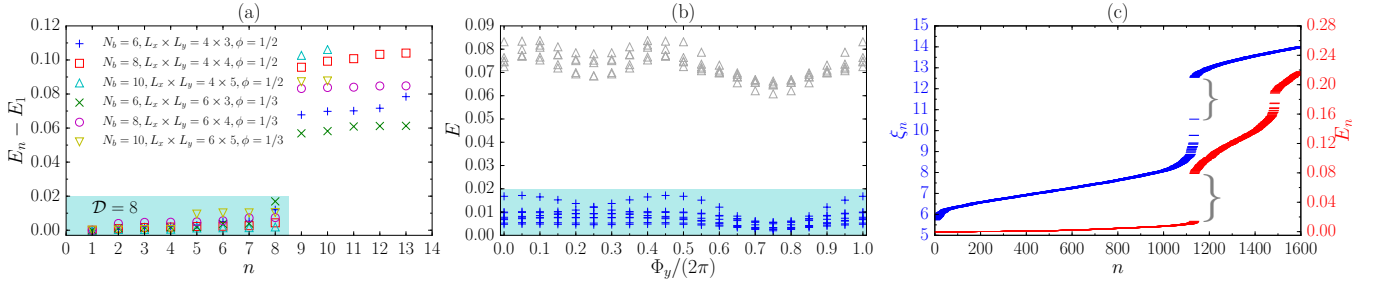


Figure 3. **Defect-enhanced topological degeneracy for Abelian systems at $\nu = 1/2$.** Two branch cuts are located at $(0.5, 0.25 \rightarrow 1.75)$, $(2.5, 0.25 \rightarrow 1.75)$ for $L_x \times L_y = 4 \times 3$; $(0.5, 0.5 \rightarrow 2.5)$, $(2.5, 0.5 \rightarrow 2.5)$ for $L_x \times L_y = 4 \times 4$ and 4×5 ; $(0.25, 0.25 \rightarrow 1.75)$, $(3.25, 0.25 \rightarrow 1.75)$ for $L_x \times L_y = 6 \times 3$; $(0.25, 0.5 \rightarrow 2.5)$, $(3.25, 0.5 \rightarrow 2.5)$ for $L_x \times L_y = 6 \times 4$; and $(0.25, 0.75 \rightarrow 3.25)$, $(3.25, 0.75 \rightarrow 3.25)$ for $L_x \times L_y = 6 \times 5$. (a) The energy spectra of various system sizes. The eight quasi-degenerate ground states are highlighted by the cyan shade. (b) The y -direction spectral flow for $N_b = 6$, $L_x \times L_y = 4 \times 3$, $\phi = 1/2$. The eight ground states (blue +) never mix with excited states (gray Δ). (c) The PES (blue) for $N_b = 8$, $L_x \times L_y = 6 \times 4$, $\phi = 1/3$ in the $N_b^A = 4$ sector and the corresponding quasihole excitations (red) for $N_b = 4$, $L_x \times L_y = 6 \times 4$, $\phi = 1/3$. The number of states below the gaps (indicated by gray $\}$) are identical in both spectra.

eigenstates. More precisely, in the presence of M pairs of defects, Eq. (2) requires us to flatten the energy dispersion of the lowest $N_s = 2N_b/k + M = 2\phi L_x L_y + M$ eigenstates of H_0 . This can be readily achieved by local perturbations owing to the strong localization of the ingap states near the defects [Fig. 2(a)]. A simple candidate of such a local potential is $V = -\sum_{n=1}^{2\phi L_x L_y + M} \epsilon_n \mathcal{T}_R(|\psi_n\rangle\langle\psi_n|)$, where ϵ_n 's and ψ_n 's are the eigenvalues and eigenvectors of H_0 respectively, and \mathcal{T}_R is the truncation at a radius R around each defect. The dominant terms in V exactly correspond to the localized eigenstates of H_0 whose energy dispersion we want to flatten, because other eigenstates staying at $\epsilon_n = 0$ have no contributions to V . This flattening process by V is asymptotically exact in the sense that the lowest $2\phi L_x L_y + M$ eigenstates of $H_0 + V$ at $R \rightarrow \infty$ will become exactly degenerate again at zero energy and have the same eigenvectors as those of H_0 . Remarkably, a very small R is already sufficient to do the flattening very well, with negligible influence on the pertinent eigenvector subspace. In Fig. 2(c), we show the band structure $\{\epsilon_n^R\}$ of $H_0 + V$ with $M = 1$ and $R = 0, 1, 2$ respectively. The degeneracy between the lowest $2\phi L_x L_y + M$ energy levels indeed becomes better with the increase of R , with the flatness $(\epsilon_{2\phi L_x L_y + M + 1}^R - \epsilon_{2\phi L_x L_y + M}^R) / (\epsilon_{2\phi L_x L_y + M}^R - \epsilon_1^R)$ significantly increased to ≈ 9.4 for $R = 2$. The corresponding eigenvectors of $H_0 + V$ have a total 99% overlap with those of H_0 for $R = 1$ and $R = 2$.

After ensuring that a suitably defined new lowest flat band can be recovered, we are now in the position to examine whether interactions can stabilize the \mathcal{Z}_k RR states in the single high-genus surfaces created in our model, by tracking the evolution of ground-state degeneracy \mathcal{D} with g . We first consider the most realistic $k = 1$ case. In the absence of defects, the ground state is two copies of $\nu = 1/2$ Laughlin states on the torus with degeneracy $\mathcal{D} = 2 \times 2 = 4$. After adding one pair of defects, we again get four-fold ground-state degeneracy, which is consistent with the $\nu = 1/2$ Laughlin state on a single $g = 2$ surface. A nontrivial enhancement of the

topological degeneracy from $\mathcal{D} = 4$ to $\mathcal{D} = 8$ occurs for two pairs of defects ($g = 3$), characterized by eight approximately degenerate ground states at the bottom of many-body energy spectra for various system sizes [Fig. 3(a)]. These states are separated from other excited states by an energy gap which is significantly larger than the ground-state splitting, and their degeneracy becomes better for larger systems. We confirm the robustness of the topological degeneracy by the spectral flow [Fig. 3(b)]: one can see that the eight ground states never mix with other excited states under twisted boundary conditions with the boundary phase. In order to further corroborate the topological nature of these ground states, we compute their particle entanglement spectra (PES) [22, 23] to probe the quasihole excitation property. We do find a clear gap in the PES, the number of states below which is exactly the same as the counting of corresponding quasihole excitations [Fig. 3(c)]. Our evidence unambiguously indicates that the ground state in the presence of M pairs of defects is the $\nu = 1/2$ Laughlin state on a single $g = M + 1$ surface with degeneracy $\mathcal{D}_M^{k=1} = 2^{M+1}$. Note also that the splitting of low-lying ‘‘genon’’ states is reduced relative to the excitation gap as the system size—and thus the separation of genons—is increased.

The effect of defects is even more intriguing at higher k 's for which host systems have intrinsic non-Abelian topological orders. In this case, unlike the situation with $k = 1$, one pair of defects can already lead to a nontrivial enhancement of the ground-state degeneracy. For example, in the case of $k = 2$, the ground state in the absence of defects is two copies of Moore-Read states on the torus, with a degeneracy $\mathcal{D} = 9$ for even $N_b/2$ and $\mathcal{D} = 1$ for odd $N_b/2$. Strikingly, after adding only one pair of defects, we observe an enhanced topological degeneracy of ten-fold for all even N_b , which becomes better for larger system sizes and is robust under twisted boundary conditions [Figs. 4(a) and (c)]. By just adding another pair of defects, the ground-state degeneracy is further enhanced to $\mathcal{D} = 36$ [Figs. 4(b) and (d)], with a faster growth rate than

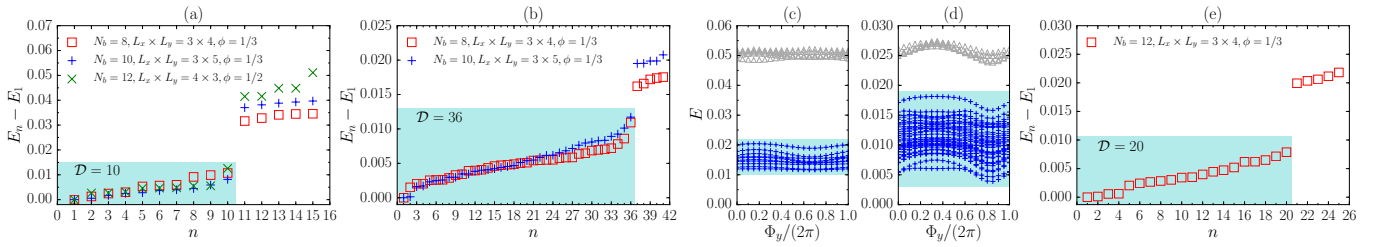


Figure 4. Defect-enhanced topological degeneracy for non-Abelian systems. The approximately degenerate ground states, together with the degeneracy \mathcal{D} , are highlighted by the cyan shade. (a) The energy spectra at $\nu = 1$ with one pair of defects. The branch cut is located at $(0.5, 0.5 \rightarrow 2.5)$ for $L_x \times L_y = 3 \times 4$; $(0.5, 0.75 \rightarrow 3.25)$ for $L_x \times L_y = 3 \times 5$; and $(1.5, 0.25 \rightarrow 1.75)$ for $L_x \times L_y = 4 \times 3$. (b) The energy spectra at $\nu = 1$ with two pairs of defects. The branch cuts are located at $(0.25, 0.5 \rightarrow 2.5)$, $(1.75, 0.5 \rightarrow 2.5)$ for $L_x \times L_y = 3 \times 4$ and $(0.25, 0.75 \rightarrow 3.25)$, $(1.75, 0.75 \rightarrow 3.25)$ for $L_x \times L_y = 3 \times 5$. (c) The y -direction spectral flow for $N_b = 10$, $L_x \times L_y = 3 \times 5$, $\phi = 1/3$ with the same branch cut as in (a). (d) The y -direction spectral flow for $N_b = 10$, $L_x \times L_y = 3 \times 5$, $\phi = 1/3$ with the same branch cuts as in (b). (e) The energy spectrum at $\nu = 3/2$ with one pair of defects. The branch cut is located at $(0.25, 0.5 \rightarrow 2.5)$ for $L_x \times L_y = 3 \times 4$.

the $k = 1$ case. The dependence of topological degeneracy on the number of defects convincingly suggests that, by introducing M pairs of defects for $k = 2$, we indeed realize the $\nu = 1$ Moore-Read state on a single $g = M + 1$ surface with degeneracy $\mathcal{D}_M^{k=2} = 2^M(2^{M+1} + 1)$ [24]. A similar enhancement of the topological degeneracy is also observed for $k = 3$, where the ground-state degeneracy is increased from $\mathcal{D} = 16$ to $\mathcal{D} = 20$ by adding $M = 1$ pair of defects [Figs. 4(e)], which is consistent with the $\nu = 3/2$ \mathcal{Z}_3 RR state on a single $g = M + 1$ surface with degeneracy $\mathcal{D}_M^{k=3} = 2[(5 + \sqrt{5})^M + (5 - \sqrt{5})^M]$ [24].

The enhanced topological degeneracy strongly indicates that the defects in our systems can indeed be thought of as genons. In particular, each genon (or defect) in our model carries a distinct nontrivial quantum dimension $d = \lim_{M \rightarrow \infty} (\mathcal{D}_M)^{\frac{1}{2M}}$, i.e., its average contribution to the total degeneracy in the thermodynamic limit, from the intrinsic quasiparticle of the corresponding host state. For example, we have non-Abelian genons with $d = \sqrt{2}$ at $\nu = 1/2$, although the Laughlin state only has Abelian quasiparticles. More saliently, genons at $\nu = 1$ in our model have $d = 2$ thus allowing for universal quantum computation, while the quasiparticles of Moore-Read state itself cannot. Moreover, we obtain genons with even higher quantum dimension $d = \sqrt{5 + \sqrt{5}}$ at $\nu = 3/2$. These differences, together with the distinctive projective braiding statistics of defects [14], imply the possibility that defects are more powerful tools for topological quantum computation than ordinary quasiparticles.

The key ingredients of our proposal are already experimentally available and their combined synthesis is plausibly within reach—especially for coupled Laughlin states emerging from a particularly simple onsite two-body interaction. Artificial gauge fields generated by lattice shaking techniques are compatible with multiple internal degrees of freedom as we require. The long-range hopping, which is chosen for theoretical elegance and numerical efficiency, is in fact not essential for the existence of lattice genons as we demonstrate in the Appendix. Hence the already realized Hofstadter model in optical lattices [25, 26] can serve as an eminently promising

candidate platform for creating genons, while its higher Chern bands provide an additional variety of host quantum Hall liquids [27]. In particular, a recent realization [28] based on a quantum gas microscope already allows single-site addressing, and could be combined with holographic beam shaping methods [29] that provide a natural route towards producing the branch cuts and local potentials necessary to realize lattice genons as we envision.

ACKNOWLEDGEMENTS

We thank N.R. Cooper and J. Behrmann for useful discussions. Z.L. was supported by Alexander von Humboldt Research Fellowship for Postdoctoral Researchers and the US Department of Energy, Office of Basic Energy Sciences through Grant No. DE-SC0002140. The latter was specifically for the use of computational facilities at Princeton University. G.M. is supported by The Royal Society – Grant No. UF120157, and acknowledges use of the Darwin Supercomputer of the University of Cambridge High Performance Computing Service, funded by Strategic Research Infrastructure Funding from the Higher Education Funding Council for England and funding from the Science and Technology Facilities Council. E.J.B. was supported by the Swedish research council (VR) and the Wallenberg Academy Fellows program of the Knut and Alice Wallenberg Foundation.

APPENDIX

Tight-binding Hamiltonian

Our model is on a two-dimensional square lattice spanned by unit vectors \mathbf{e}_x and \mathbf{e}_y in the x - and y -direction. The single-particle tight-binding Hamiltonian can be written as

$$H_0 = \sum_{j,k,\sigma} t(z_j, z_k) a_{j, \mathcal{F}^{n_{jk}}(\sigma)}^\dagger a_{k,\sigma}, \quad (\text{A1})$$

where $a_{j,\sigma}^\dagger$ ($a_{j,\sigma}$) creates (annihilates) a particle in layer σ at lattice site j with coordinate $z_j = x_j \mathbf{e}_x + y_j \mathbf{e}_y$, and $\mathcal{F}^{n_{jk}}(\sigma)$ flips σ for n_{jk} times if the hopping from z_k to z_j intersects with n_{jk} branch cuts. The hopping coefficient from z_k to z_j is designed as $t(z_j, z_k) = (-1)^{x+y+xy} e^{-\frac{\pi}{2}(1-\phi)|z|^2} e^{-i\pi\phi(x_j+x_k)y}$ [17], where $z = z_j - z_k = x\mathbf{e}_x + y\mathbf{e}_y$. Such a hopping is local in the sense that $t(z_j, z_k)$ follows a super-exponential decay. We focus on $\phi = 1/q$ with integer q , for which a unit cell contains q sites in the x -direction. In the absence of defects, H_0 has a Z_2 symmetry associated with exchanging the two layers and corresponds to two decoupled Kapit-Mueller models [17] in the Landau gauge, thus its lowest band structure contains two copies of an exactly flat band at zero energy with Chern number $\mathcal{C} = 1$.

In a finite system with periodic boundary conditions, both the lattice sites and defects appear periodically. To adjust Eq. (A1) to periodic boundary conditions, we replace $t(z_j, z_k)$ by $\sum_{s,t=-\infty}^{+\infty} t(z_j + sL_x \mathbf{e}_x + tL_y \mathbf{e}_y, z_k) e^{2\pi i s L_x y_j \phi}$, and in n_{jk} we count all crossings between the hopping from z_k to $z_j + sL_x \mathbf{e}_x + tL_y \mathbf{e}_y$ and the periodically appearing branch cuts. We arrange the branch cuts in the y -direction (see Appendix ‘Tilted branch cuts’), and keep defects well separated from each other. We avoid overlaps between branch cuts and lattice sites. We also pursue a good separation of scales in the many-body spectrum when we choose the locations of defects. However, we emphasize that our results are not sensitive to the precise locations of defects or the arrangement of branch cuts and crucially also hold for models including only short-range hopping once the system size is large enough.

Derivation of Eq. (2)

For a fractional quantum Hall state at filling fraction ν in the lowest Landau level on a surface of genus g , the following relation holds:

$$N_\phi = N/\nu - \mathcal{S}_g, \quad (\text{A2})$$

where N_ϕ is the number of magnetic flux quanta penetrating the surface, N is the number of particles, and \mathcal{S}_g is the so-called topological shift. Chern-Simons theory tells us $\mathcal{S}_g = \mathcal{S}_{g=0} \times (1-g)$ [21]. Furthermore, the number of single-particle states N_s in the lowest Landau level is related to N_ϕ by $N_s = N_\phi + 1 - g$ [20]. Because $\mathcal{S}_{g=0} = 2$ for $\nu = k/2$

Z_k bosonic RR states, we have $\mathcal{S}_g = 2(1-g)$. Consequently, Eq. (A2) can be written as $N_s - (1-g) = 2N/k - 2(1-g)$, leading to $N_s = 2N/k - (1-g)$ for $\nu = k/2$ Z_k bosonic RR states as shown in Eq. (2).

Projected interaction

In the presence of M pairs of defects, we showed that the energy dispersion of the lowest $2\phi L_x L_y + M$ eigenstates of H_0 can be flattened by local potentials with a negligible influence on the subspace of eigenvectors. Hence, we can safely project the interaction H_{int} , which is assumed to be small relative to the band gap, to these eigenstates and neglect their energy dispersion for large numerical efficiency. This procedure is similar to the band projection in the flat-band limit which has been extensively used in previous studies of fractional Chern insulators without defects [23]. Taking the two-body on-site interaction as an example, the interaction after projection is

$$H_{\text{int}}^{\text{proj}} = \sum_{m_1, m_2, m_3, m_4=1}^{2\phi L_x L_y + M} C_{m_1, m_2, m_3, m_4} a_{m_1}^\dagger a_{m_2}^\dagger a_{m_3} a_{m_4},$$

$$C_{m_1, m_2, m_3, m_4} = \sum_{i=1}^{2L_x L_y} \psi_{m_1, i}^* \psi_{m_2, i}^* \psi_{m_3, i} \psi_{m_4, i}, \quad (\text{A3})$$

where a_m^\dagger (a_m) creates (annihilates) a boson on the eigenstate ψ_m of H_0 , and $\psi_m = (\psi_{m,1}, \dots, \psi_{m,2L_x L_y})$ in the lattice site basis $a_{j,\sigma}^\dagger |\text{vacuum}\rangle$.

Twisted boundary conditions

For a state Ψ of N particles on a $L_x \times L_y$ lattice, twisted boundary conditions mean $\Psi(z_1, \dots, z_j + L_x \mathbf{e}_x, \dots, z_N) = e^{i\Phi_x(y)} \Psi(z_1, \dots, z_j, \dots, z_N)$, where $\Phi_x(y)$ is the boundary phase. This can be implemented by replacing $t(z_j, z_k)$ by $\sum_{s,t=-\infty}^{+\infty} t(z_j + sL_x \mathbf{e}_x + tL_y \mathbf{e}_y, z_k) e^{2\pi i s L_x y_j \phi} e^{i s \Phi_x} e^{i t \Phi_y}$ in Eq. (A1).

Particle entanglement spectrum (PES)

For a \mathcal{D} -fold degenerate ground-state manifold $\{|\Psi_\alpha\rangle\}$ of N particles, we define the PES levels ξ as $\xi \equiv -\ln \lambda$, where the λ 's are the eigenvalues of the reduced density matrix ρ_A of N_A particles obtained by tracing out $N_B = N - N_A$ particles from the whole system, i.e., $\rho_A = \text{Tr}_B \rho$ with $\rho = \frac{1}{\mathcal{D}} \sum_{\alpha=1}^{\mathcal{D}} |\Psi_\alpha\rangle \langle \Psi_\alpha|$. A gap in the PES is expected, below which the number of PES levels is the same as the counting of the corresponding quasihole excitation spectrum [23], which in our case can be obtained from diagonalizing the interaction Hamiltonian of N_b^A particles on the same lattice size.

Short-range hopping

In the main text, we use a tight-binding Hamiltonian with local but long-range hopping for theoretical elegance. Now we show that we can obtain similar results with only short-range hopping.

We only keep the nearest-neighbor and next-nearest-neighbor hopping in the tight-binding model which we use in the main text. So now we have a new tight-binding model with short-range hopping

$$H'_0 = \sum_{j,k,\sigma} t'(z_j, z_k) a_{j, \mathcal{F}^{n_{jk}(\sigma)}}^\dagger a_{k,\sigma}, \quad (\text{A4})$$

where $t'(z_j, z_k) = (-1)^{x+y+xy} e^{-\frac{\pi}{2}(1-\phi)|z|^2} e^{-i\pi\phi(x_j+x_k)y}$ for $|z|^2 \leq 2$ and $t'(z_j, z_k) = 0$ for $|z|^2 > 2$. The meanings of the symbols are the same as those in the main text.

Although the exact flatness of the lowest $2\phi L_x L_y$ eigenstates in the absence of defects is lost due to the hopping truncation, we still find that defects have almost the same effect on the band structure of H'_0 as that on H_0 shown in the main text [Figs. A1 and A2]. The energies of some eigenstates localized near the defects deviate from the original bands, and the dispersion of the lowest $2\phi L_x L_y + M$ eigenstates can be reduced by a local potential $V = -\sum_{n=1}^{2\phi L_x L_y + M} \epsilon_n \mathcal{T}_R(|\psi_n\rangle\langle\psi_n|)$, where ϵ_n 's and ψ_n 's are now the eigenvalues and eigenvectors of H'_0 respectively. One can notice that such a flattening procedure works better for smaller ϕ [Figs. A1 and A2].

We diagonalize the interaction projected onto the lowest $2\phi L_x L_y + M$ eigenstates of H'_0 to examine the topological degeneracy at various filling fractions. Strikingly, we can get the expected topological degeneracy even though we have truncated the hopping (Fig. A3). Moreover, we find that the eight-fold Laughlin degeneracy remain stable for small ϕ even if we further truncate the hopping range to only the nearest-neighbor (i.e., the conventional Hofstadter model) (Fig. A4). These results imply that the long-range hopping is not necessary for the realization of lattice genons, thus facilitating their experimental realization. A realization based on the nearest-neighbor Hofstadter model would provide an additional range of states to explore, as single layers can be chosen to realize higher Chern number bands supporting a range of hierarchy states at different filling factors [27].

Tilted branch cuts

In the main text, we arrange branch cuts in the y -direction. Now we consider locations of defects with tilted branch cuts. In general, we denote the branch cut connecting a pair of defects at (X_1, Y_1) and (X_2, Y_2) as $(X_1, Y_1) \rightarrow (X_2, Y_2)$. In the following we use the same tight-binding model H_0 as in the main text.

With tilted branch cuts, we observe a similar effect of defects on the band structure as that in the main text (Fig. A5). Moreover, the many-body spectra reproduce the expected

topological degeneracy for the given number of branch cuts (Fig. A6).

* Corresponding author: G.Moller@kent.ac.uk

- [1] X. G. Wen, *Vacuum degeneracy of chiral spin states in compactified space*, *Phys. Rev. B* **40**, 7387(R) (1989).
- [2] X. G. Wen and Q. Niu, *Ground-state degeneracy of the fractional quantum Hall states in the presence of a random potential and on high-genus Riemann surfaces*, *Phys. Rev. B* **41**, 9377 (1990).
- [3] R. B. Laughlin, *Anomalous Quantum Hall Effect: An Incompressible Quantum Fluid with Fractionally Charged Excitations*, *Phys. Rev. Lett.* **50**, 1395 (1983).
- [4] M. Oshikawa and T. Senthil, *Fractionalization, Topological Order, and Quasiparticle Statistics*, *Phys. Rev. Lett.* **96**, 060601 (2006).
- [5] X. G. Wen, *Topological orders and Chern-Simons theory in strongly correlated quantum liquid*, *Int. J. Mod. Phys. B*, **05**, 1641 (1991).
- [6] G. Moore and N. Read, *Nonabelions in the fractional quantum hall effect*, *Nucl. Phys. B* **360**, 362 (1991).
- [7] A. Kitaev, *Anyons in an exactly solved model and beyond*, *Ann. Phys.* **321**, 2 (2006).
- [8] L. Balents, *Spin liquids in frustrated magnets*, *Nature* **464**, 199 (2010).
- [9] J. Maciejko and G. A. Fiete, *Fractionalized topological insulators*, *Nat. Phys.*, **11**, 385 (2015).
- [10] M. Dolev, M. Heiblum, V. Umansky, A. Stern and D. Mahalu, *Observation of a quarter of an electron charge at the $\nu = 5/2$ quantum Hall state*, *Nature* **452**, 829 (2008).
- [11] A. Y. Kitaev, *Fault-tolerant quantum computation by anyons*, *Ann. Phys.* **303**, 2 (2003).
- [12] C. Nayak, S. H. Simon, A. Stern, M. Freedman, and S. Das Sarma, *Non-Abelian anyons and topological quantum computation*, *Rev. Mod. Phys.* **80**, 1083 (2008).
- [13] M. Barkeshli and X.-L. Qi, *Topological Nematic States and Non-Abelian Lattice Dislocations*, *Phys. Rev. X* **2**, 031013 (2012).
- [14] M. Barkeshli, C.-M. Jian, and X.-L. Qi, *Twist defects and projective non-Abelian braiding statistics*, *Phys. Rev. B* **87**, 045130 (2013).
- [15] S. A. Parameswaran, R. Roy, and S. L. Sondhi, *Fractional quantum Hall physics in topological flat bands*, *C. R. Physique* **14**, 816 (2013).
- [16] E.J. Bergholtz and Z. Liu, *Topological Flat Band Models and Fractional Chern Insulators*, *Int. J. Mod. Phys. B* **27**, 1330017 (2013).
- [17] E. Kapit and E. Mueller, *Exact Parent Hamiltonian for the Quantum Hall States in a Optical Lattice*, *Phys. Rev. Lett.* **105**, 215303 (2010).
- [18] Z. Liu, E. J. Bergholtz and E. Kapit, *Non-Abelian fractional Chern insulators from long-range interactions*, *Phys. Rev. B* **88**, 205101 (2013).
- [19] J. Behrmann, Z. Liu, and E.J. Bergholtz, *Model Fractional Chern Insulators*, *Phys. Rev. Lett.* **116**, 216802.
- [20] R. Alicki, J. R. Klauder, and J. Lewandowski, *Landau-level ground-state degeneracy and its relevance for a general quantization procedure*, *Phys. Rev. A* **48**, 2538 (1993).
- [21] E. Ardonne, *A conformal field theory description of fractional quantum Hall states*, Ph.D. thesis, 2002.

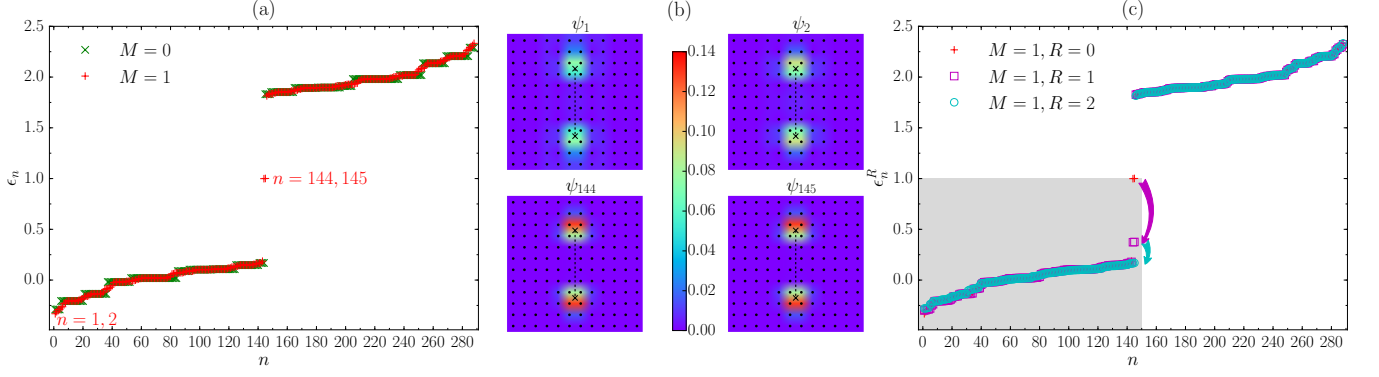


Figure A1. We study the band structure on a $L_x \times L_y = 12 \times 12$ lattice with $\phi = 1/2$. (a) The single-particle spectrum $\{\epsilon_n\}$ of H'_0 . In the absence of defects ($M = 0$), $\epsilon_1, \dots, \epsilon_{144}$ are no longer exactly degenerate at zero energy. With one pair of defects ($M = 1$) at $(5.5, 2.5 \rightarrow 8.5)$, the original band structure is distorted, with one nearly degenerate cluster ($\epsilon_{144}, \epsilon_{145}$) having the largest deviation. (b) The lattice site weight of eigenvectors $\psi_1, \psi_2, \psi_{144}, \psi_{145}$ of H'_0 for the same defects as in (a). All of them are strongly localized near the defects. However, the localization of ψ_1 and ψ_2 is weaker than the case of H_0 in the main text, probably because now they have much less energy deviation from the original band structure. (c) The single-particle spectrum $\{\epsilon_n^R\}$ of $H'_0 + V$ with $R = 0, 1$, and 2 and the same defects as in (a). The degeneracy of $\epsilon_1^R, \dots, \epsilon_{145}^R$ (shaded in gray) becomes better for larger R , with the flatness $0.6, 2.2, 3.7$ for $R = 0, 1, 2$.

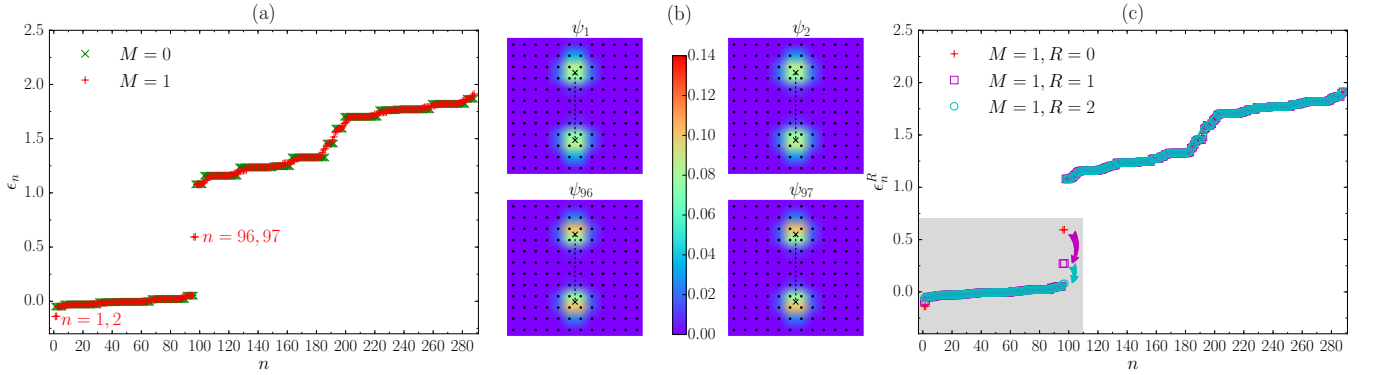


Figure A2. We study the band structure on a $L_x \times L_y = 12 \times 12$ lattice with $\phi = 1/3$. (a) The single-particle spectrum $\{\epsilon_n\}$ of H'_0 . In the absence of defects ($M = 0$), $\epsilon_1, \dots, \epsilon_{96}$ are no longer exactly degenerate at zero energy. With one pair of defects ($M = 1$) at $(5.5, 2.5 \rightarrow 8.5)$, the original band structure is distorted, with two nearly degenerate clusters (ϵ_1, ϵ_2) and ($\epsilon_{96}, \epsilon_{97}$) having the largest deviation. (b) The lattice site weight of eigenvectors $\psi_1, \psi_2, \psi_{96}, \psi_{97}$ of H'_0 for the same defects as in (a). All of them are strongly localized near the defects. (c) The single-particle spectrum $\{\epsilon_n^R\}$ of $H'_0 + V$ with $R = 0, 1$, and 2 and the same defects as in (a). The degeneracy of $\epsilon_1^R, \dots, \epsilon_{97}^R$ (shaded in gray) becomes better for larger R , with the flatness $0.7, 2.2, 7.3$ for $R = 0, 1, 2$.

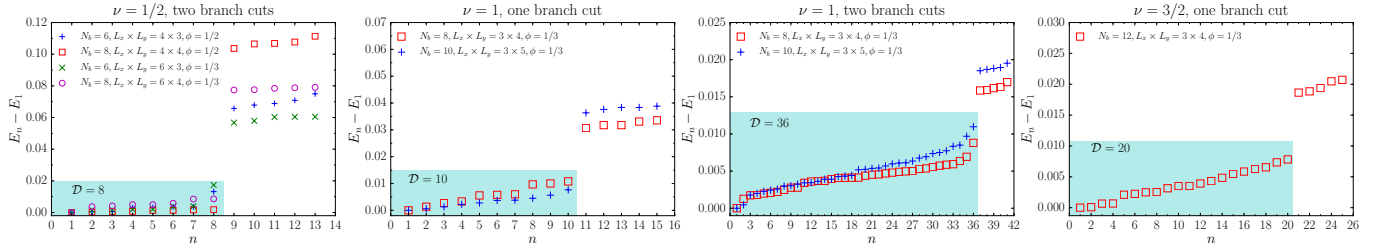


Figure A3. We repeat the many-body calculations with the single-particle Hamiltonian H'_0 . The interactions and branch cut locations in each specific system size are the same as those used in the main text with H_0 . The approximately degenerate ground states, together with the degeneracy D , are highlighted by the cyan shade. One can notice that we get the same topological degeneracy as that in the main text.

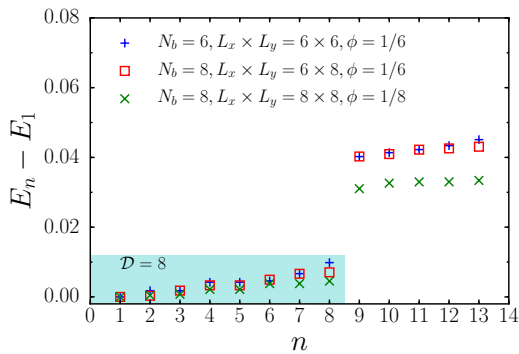


Figure A4. We do the many-body calculations with the Hofstadter single-particle Hamiltonian for two branch cuts at $\nu = 1/2$. Two branch cuts are located at $(0.25, 0.5 \rightarrow 3.5)$, $(3.25, 0.5 \rightarrow 3.5)$ for $L_x \times L_y = 6 \times 6$; $(0.25, 1.5 \rightarrow 5.5)$, $(3.25, 1.5 \rightarrow 5.5)$ for $L_x \times L_y = 6 \times 8$; and $(1.5, 1.5 \rightarrow 5.5)$, $(5.5, 1.5 \rightarrow 5.5)$ for $L_x \times L_y = 8 \times 8$.

[22] A. Sterdyniak, N. Regnault, and B. A. Bernevig, *Extracting Excitations from Model State Entanglement*, *Phys. Rev. Lett.* **106**, 100405 (2011).

[23] N. Regnault and B. A. Bernevig, *Fractional Chern Insulator*, *Phys. Rev. X* **1**, 021014 (2011).

[24] E. Ardonne, E. Bergholtz, J. Kailasvuori, and E. Wikberg, *Degeneracy of non-Abelian quantum Hall states on the torus: domain walls and conformal field theory*, *J. Stat. Mech.* P04016 (2008).

[25] M. Aidelsburger, M. Atala, M. Lohse, J. T. Barreiro, B. Paredes, and I. Bloch, *Realization of the Hofstadter Hamiltonian with Ultracold Atoms in Optical Lattices*, *Phys. Rev. Lett.* **111**, 185301 (2013).

[26] H. Miyake, G. A. Siviloglou, C. J. Kennedy, W. C. Burton, and W. Ketterle, *Realizing the Harper Hamiltonian with Laser-Assisted Tunneling in Optical Lattices*, *Phys. Rev. Lett.* **111**, 185302 (2013).

[27] G. Möller, N. R. Cooper, *Fractional Chern Insulators in Harper-Hofstadter Bands with Higher Chern Number*, *Phys. Rev. Lett.* **115**, 126401 (2015).

[28] M. E. Tai, A. Lukin, M. Rispoli, R. Schittko, T. Menke, D. Borgnia, P. M. Preiss, F. Grusdt, A. M. Kaufman, M. Greiner, *Microscopy of the interacting Harper-Hofstadter model in the few-body limit*, [arXiv:1612.05631](https://arxiv.org/abs/1612.05631).

[29] P. Zupancic, P. M. Preiss, R. Ma, A. Lukin, M. E. Tai, M. Rispoli, R. Islam, and M. Greiner, *Ultra-precise holographic beam shaping for microscopic quantum control*, *Opt. Express* **24**, 13881 (2016).

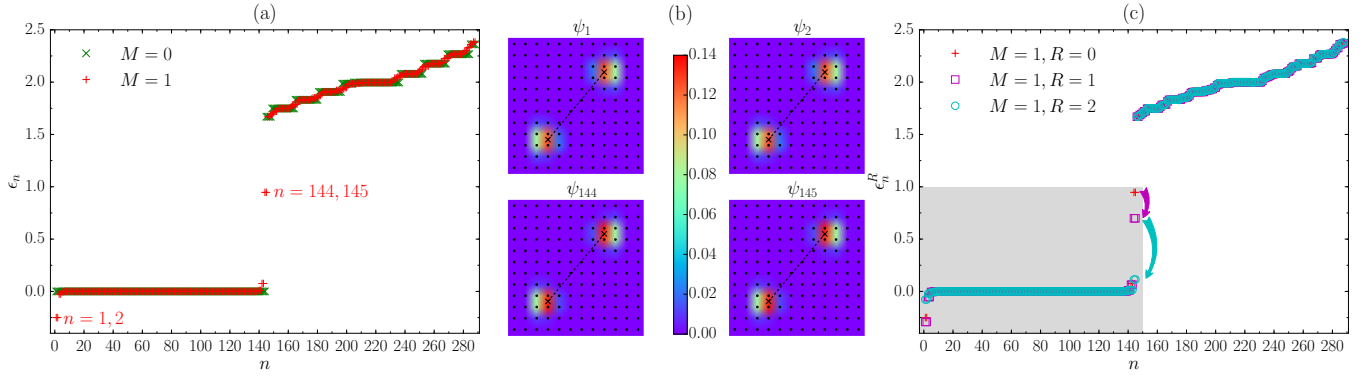


Figure A5. We study the band structure on a $L_x \times L_y = 12 \times 12$ lattice with $\phi = 1/2$. (a) The single-particle spectrum $\{\epsilon_n\}$ of H_0 . In the absence of defects ($M = 0$), $\epsilon_1, \dots, \epsilon_{144}$ are exactly degenerate at zero energy. With one tilted branch cut ($M = 1$) at $(3, 2.5) \rightarrow (8, 8.5)$, the original band structure is distorted, with two nearly degenerate clusters (ϵ_1, ϵ_2) and $(\epsilon_{144}, \epsilon_{145})$ having the largest deviation. (b) The lattice site weight of eigenvectors $\psi_1, \psi_2, \psi_{144}, \psi_{145}$ of H_0 for the same defects as in (a). All of them are strongly localized near the defects. The eigenstates with less energy deviation from the original band structure, for example, $\psi_3, \psi_4, \psi_{142}, \psi_{143}$, are less localized (not shown here). (c) The single-particle spectrum $\{\epsilon_n^R\}$ of $H_0 + V$ with $R = 0, 1$, and 2 and the same defects as in (a). The degeneracy of $\epsilon_1^R, \dots, \epsilon_{145}^R$ (shaded in gray) becomes better for larger R , with the flatness $0.6, 1.0, 8.1$ for $R = 0, 1, 2$.

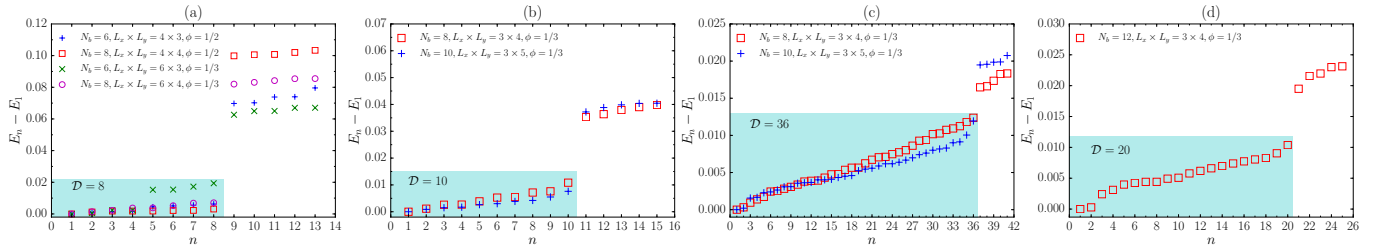


Figure A6. The many-body spectra with tilted branch cuts. The approximately degenerate ground states, together with the degeneracy \mathcal{D} , are highlighted by the cyan shade. (a) $\nu = 1/2$ with two branch cuts at $(0.25, 0.5) \rightarrow (0.5, 2), (2.25, 0) \rightarrow (2.5, 1.5)$ for $L_x \times L_y = 4 \times 3$; $(0, 0.75) \rightarrow (1, 2.75), (2, 0.25) \rightarrow (3, 2.25)$ for $L_x \times L_y = 4 \times 4$; $(0.25, 0.5) \rightarrow (0.5, 2), (3.25, 0) \rightarrow (3.5, 1.5)$ for $L_x \times L_y = 6 \times 3$; and $(0.5, 0.75) \rightarrow (1.5, 2.75), (3.5, 0.25) \rightarrow (4.5, 2.25)$ for $L_x \times L_y = 6 \times 4$. (b) $\nu = 1$ with one branch cut at $(0.25, 0.5) \rightarrow (1.75, 2.5)$ for $L_x \times L_y = 3 \times 4$ and $(0.25, 0.5) \rightarrow (1.75, 3)$ for $L_x \times L_y = 3 \times 5$. (c) $\nu = 1$ with two branch cuts at $(0.1, 0.75) \rightarrow (0.4, 2.75), (1.6, 0.25) \rightarrow (1.9, 2.25)$ for $L_x \times L_y = 3 \times 4$ and $(0.19, 0.5) \rightarrow (0.31, 3.5), (1.69, 0.45) \rightarrow (1.81, 3.45)$ for $L_x \times L_y = 3 \times 5$. (d) $\nu = 3/2$ with one branch cut at $(0.5, 0.5) \rightarrow (2, 2.5)$ for $L_x \times L_y = 3 \times 4$.